Ceramics International xxx (xxxx) xxx

Contents lists available at ScienceDirect

Ceramics International

journal homepage: www.elsevier.com/locate/ceramint

Effect of microstructure on the physicochemical characteristics of foam glass made by soda lime -CRT glasses and aluminium dross

Meriem Sassi [a,*], Andrea Simon [b], Sindy Fuhrmann [d], Stephan A.H. Sander [d], Roland Szabó [c]

[a] Karlsruhe Institute of Technology, Institute for Technical Chemistry (ITC), Hermann-von-Helmholtz-Platz 1, 76344, Eggenstein-Leopoldshafen, Germany
[b] Institute of Ceramics and Polymer Engineering, University of Miskolc, H-3515, Miskolc-Egyetemváros, Hungary
[c] Institute of Raw Material Preparation and Environmental Technology, University of Miskolc, H-3515, Miskolc-Egyetemváros, Hungary
[d] Institut für Glas und Glastechnologie, Erich-Rammler-Bau, Leipziger Straße 28, Freiberg, Germany

ARTICLE INFO

Handling Editor: Dr P. Vincenzini

Keywords:
Aluminium dross
Soda lime glass
CRT glass
Computed tomography
Foam glass

ABSTRACT

Foam glass, an inorganic insulation material, is primarily manufactured from recycled glass or sand combined with a foaming agent. During fabrication, gas bubbles are generated in the softened glass, causing it to expand and form a cellular structure. Critical parameters such as cell size, type (closed or open cells), distribution, and uniformity significantly influence the physical and chemical properties of foam glass, ensuring sustained thermal efficiency. This research aims to produce foam glass exclusively from waste materials, thereby promoting the circular economy by utilizing container glass, cathode ray tube (CRT) glass, and aluminium dross. A comprehensive microstructural analysis, employing computer tomography and scanning electron microscopy, elucidated key properties including density, thermal conductivity, and water absorption. The manufactured foam glass exhibited lightweight characteristics, with a density ranging from 0.15 to 0.18 g/cm^3. Additionally, the foam glass demonstrated low thermal conductivity (between 0.038 W/m·K and 0.05 W/m·K), which can be attributed to the heterogeneous distribution of cells that effectively reduce heat convection. This property makes foam glass an excellent thermal insulator. Furthermore, both high-absorption (open porosity) and low-absorption (closed porosity) foam glasses were successfully produced.

1. Introduction

Currently, ensuring the energy efficiency of new infrastructure has become a critical issue. One promising solution is the development of effective heat-insulating materials, with foam glass emerging as a highly promising option. Foam glass features a cellular-like structure characterized by low density, excellent chemical stability, and incombustibility [1–7]. It is renowned for its application in the construction of energy-efficient Passive Houses [8,9], pavements, roads, harbor areas, bridge embankments, ramps, and culvert foundations [9,10].

The primary inconvenience of using foam glass is its high cost, which often drives customers to opt for alternative insulating materials. However, since the main component of foam glass is glass powder combined with a foaming agent [11–14], using waste materials as a substitute can help mitigate source depletion, promote the circular economy, and effectively manage waste disposal. In this contest, foam glass can be made with different waste materials such as waste glass [15–18], fly ash [19–24], wood ash [25], plaster waste [26], high titanium blast furnace slag [27,28], red mud [28,29], geopolymers [30,31].

In this study, two hazardous wastes (cathode ray tube (CRT) glass and aluminium dross) were combined with container glass to produce foam glass. CRT glass contains barium, strontium, lead, and other hazardous elements such as antimony, europium, and selenium [32–34]. Lead poses a risk of dispersing poisonous substances during the remelting process, making the recycling of CRT glass challenging and necessitating special safety measures. Addressing this issue is critical for developing effective treatment systems for Waste Electrical and Electronic Equipment (WEEE) [32]. The most effective approach is to transform CRT glass into functional materials [35–41].

A similar problem occurs with aluminium dross, a byproduct of the secondary aluminium industry during aluminium scrap processing. Aluminium dross may contain up to 30 % aluminium oxide, 30–55 % sodium chloride, 15–30 % potassium chloride, 5–7% metallic aluminium, and impurities such as carbides, nitrides, sulfides, and phosphides) [31,42–46]. Due to these impurities, it is classified as toxic

* Corresponding author.
E-mail address: sassi90meriem@gmail.com (M. Sassi).

https://doi.org/10.1016/j.ceramint.2024.07.098
Received 26 March 2024; Received in revised form 17 June 2024; Accepted 8 July 2024
Available online 9 July 2024

and hazardous waste and must be handled under specific legalization [46–48]. Pyrometallurgical and hydrometallurgical methods can be used to recycle aluminium dross [46,49–53]. However, these methods generate non-metallic waste and require additional treatment to remove aluminium nitride (AlN) [54].

The most effective way of recycling aluminium dross is to use it directly in the production of valuable products such as composites, alloys, aluminum derivative compounds, aluminium-alumina refractories, refractory coatings, cement clinker production [31,55], catalyst support for glycerol dry reforming [56], and as a partial replacement for sand in sandcrete blocks [44]. Few studies have explored the addition of aluminum dross to foam glass [1,51,57,58]. In this paper, we not only used aluminium dross but also combined it with another hazardous material (CRT glass), utilizing both in significant quantities, reaching up to 20 wt% of the overall raw material.

In conclusion, this paper demonstrates the potential of producing foam glass using 100 wt% waste materials: container glass, cathode ray tube (CRT) glass, aluminium dross, and silicon carbide. We discuss the effects of the chemical composition of these waste materials on the microstructure and characteristics of the foam by explaining the different chemical bonding taking place during foaming. This leads to establishing the relation between porosity, density, and thermal conductivity for optimal foam glass that can compete with commercial foam glass.

2. Materials and experimental procedures

2.1. Materials and sample preparation

Glass containers were collected from households in Miskolc (white glass). A process of washing, cleaning, drying, crushing, and milling was carried out on the containers. Horiba Laser Scattering Particle Size Distribution Analyzer LA-950 was used to measure the particle size of the glass powder. According to the cumulative curve, D95 corresponds to 94 μm. To reach a smaller particle size, a 63 μm sieve was used. CRT glass powder with particle size of less than 63 was supplied by Daniella Ipari Park Ltd. The aluminium dross was provided by Arconic-Köfém Mill Products Hungary Ltd., Szekesfehervar, Hungary. As received, the dross was treated to remove the metals and salt content by Kekesi et al. [59]. The process starts with melting aluminum slag to recover metals, then the remaining dross is crushed, milled, and washed with distilled water three times to remove salt content.

The chemical composition of the bottle and CRT glasses was determined by X-ray fluorescence (Rikagu Supermini, Rigaku Europe SE, Neu-Isenburg, HE, GER). The dross mineral composition was determined by X-ray powder diffractometry (XRD) (XRD,Rigaku Miniflex II, Rigaku Corporation, Tokyo, JPN)) and analyzed by Rietveld-fitting. The particle morphology of the raw materials was characterized using a scanning electron microscope (SEM) Zeiss EVO MA10 (Carl Zeiss AG, Oberkochen, BW, GER.).

The mixtures were prepared by taking container glass as the basic component and adding 10 wt% dross while varying the amount of CRT glass content (0, 5, and 10 wt%). 2 wt% silicon carbide was added as a foaming agent. 100 g of each composition were weighed and homogenized in a laboratory mixer for 10 min at 300 rpm.

Mixture foaming behavior was investigated using a heating microscope (MicrOvis, Camar Elettronica). An approximately 5 mm height and 2 mm diameter sample was pressed using the microscope mold kit and placed on an alumina sheet in the microscope furnace. The sample's silhouette changes depending on the temperature to identify the beginning of sintering, softening, sphere, half-sphere, and melting temperatures. The maximum sample height corresponds to the foaming temperature.

After determining the exact foaming temperature, 10 samples from each mixture were prepared by pouring 5 g into a stainless-steel mold and pressing under 11 MPa for 10 s into a cylindrical shape (diameter = 20 mm, height = 11 mm). In an electric chamber furnace, the samples were sintered at a heating rate of 5 °C/min and a holding time of 10 min.

Table 1
Composition of the mixtures (wt%).

Name	Dross 64	SiC	CRT	G
G	0	2	0	98
G5CRT	0	2	5	93
G10CRT	0	2	10	88
G10D64	10	2	0	88
G5CRT10D64	10	2	5	83
G10CRT10D64	10	2	10	78

In the sample coding (Table 1), G refers to the base glass, the first digit refers to the amount of CRT glass content (5 or 10 wt%) and the second digit presents the amount of aluminium dross (0 or 10 wt%). D64 is the type of dross used.

2.2. Characterization methods

After sintering, volume expansion, water absorption, bulk density, porosity, microstructure, thermal conductivity, and compressive strength were investigated.

The samples were cut into cylindrical shapes (diameter = 40 mm, height = 16.5 mm) to measure the volume expansion and the apparent density. The apparent densities of the samples were calculated as mass per volume (g/cm^3). The volume expansion coefficient was calculated as follows:

$$\textit{Volume expansion Coeff}\ (-) = (V_F - V_i) / V_i \quad (1)$$

Where: V_i and V_F are the volume of the sample before and after firing (cm^3) respectively.

Water absorption measurement was made according to method B of the Hungarian standard MSZ EN 1217 B. After boiling for 4 h in distilled water, samples were soaked for 24 h then the water absorption was calculated as follows:

$$\textit{Water absorption}\ (\%) = \frac{m_{wet} - m_{dry}}{m_{dry}} * 100 \quad (2)$$

Where: m_{dry} and m_{wet} indicate the weight of the dry sample and the weight of the soaked sample (g) respectively.

For macrostructure analysis photos of the foam glass were taken. Besides, using computerized tomography (YXLON CT computed tomography system scan), images of the foam were taken from different angles, and cross-sectional images (slices) were created without destroying the samples. For the microstructure characterization, the samples were sent to scanning electron microscopy (SEM) with a Zeiss EVO MA10 (Carl Zeiss AG, Oberkochen, BW, GER). Coating the samples with gold is required to prevent thermal damage, inhibit charging, and improve the secondary electron signal.

The porosity (open and closed pores) of the foam was determined through the measurement of the skeletal density and the powder density (ground in mortar) using a Helium pycnometer (Ultrapyc 1200e Automatic Gas Pycnometer, Quantachrome GmbH & Co. KG, Odelzhausen, BY.).

$$\phi = \left(1 - \frac{\rho_{bulk}}{\rho_{solid}}\right) \times 100 \quad (3)$$

$$\phi_{cp} = \frac{\rho_{skel}^{-1} - \rho_{solid}^{-1}}{\rho_{bulk}^{-1} - \rho_{solid}^{-1}} \times 100\ \% \quad (4)$$

The skeletal density (ρ_{skel}) is the density of the foam structure measured by the He pycnometer.

The bulk density (ρ_{bulk}) is the geometrical density calculated as the mass per volume.

The solid density (ρ_{solid}) is the density of the powder issued from

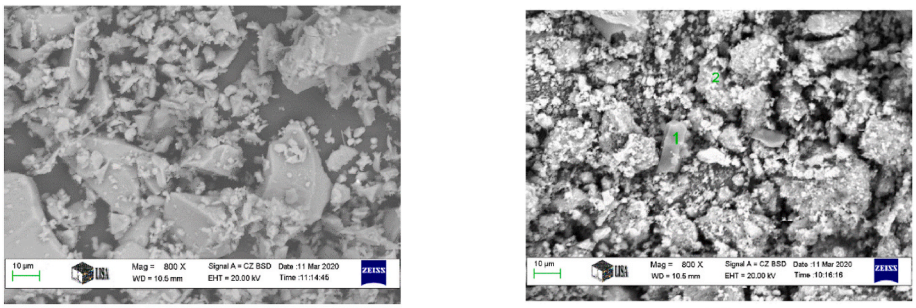

Figure 1. SEM analysis of CRT glass (A) and dross 64 (B).

Table 2
Chemical composition (wt%) of container glass (G) and CRT glass (XRF analysis).

Sample	SiO_2	Al_2O_3	MgO	CaO	Na_2O	K_2O	Fe_2O_3	F	S	MnO	TiO_2	P_2O_5
G	74.0	1.3	2.26	8.32	12.03	0.62	0.45	<0.3	0.18	0.008	0.048	0.011
CRT	53.5	1.6	0.26	0.56	5.11	5.30	0.05	<0.3	0.02	<0.005	0.317	<0.005

Table 3
Hazardous elements in CRT glass (XRF analysis, DL = detection limit)).

Element (ppm)	Cu	Zn	Pb	Rb	Sr	Ba	As	Cr	Co	Ni	Zr
CRT	14	1808	2342	<10	3.73	10.51	33	<DL	11	70	0.40 %

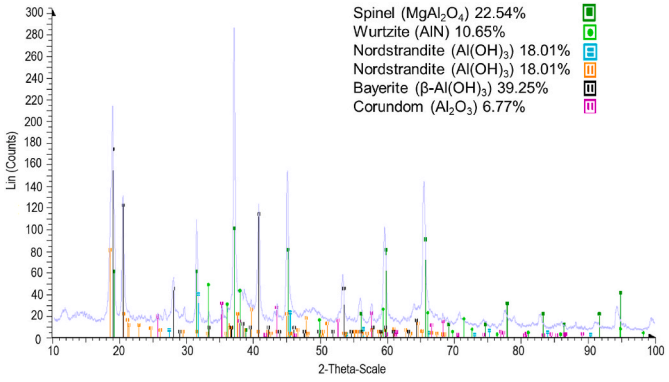

Figure 2. Mineral composition of the aluminium dross (XRD analysis).

grinding the foam glass.

The thermal conductivity was measured using a TCi thermal conductivity analyser (C-Therm Technologies Ltd., Fredericton, NB, CAN) applying the Modified Transient Plane Source Method (as per ASTM D7984) [60].

3. Results and discussion

3.1. Raw material characterization

Fig. 1 illustrates the morphology of raw materials. The CRT glass micrograph displays polyhedral shapes in the order of 20–50 μm with multiple planar faces surrounded by small debris. Similar to container glass, CRT glass is composed of silica, sodium oxide, and calcium oxide, with minor amounts of magnesium or alumina. However, it contains hazardous elements such as Pb, Sr, and Ba (Table 2, Table 3).

Aluminium dross is mainly composed of aluminium oxides and spinel in the form of round grains, whisker crystals, and a minor fraction of salt content with a rigid and rough structure. Dross mineral composition shows phases such as spinel ($MgAl_2O_4$), bayerite (β-$Al(OH)_3$, wurtzite (AlN), corundom (Al_2O_3), halite (NaCl), nordstrandite ($Al(OH)_3$) (Fig. 2). Residual salts can act as flux and reduce the foaming temperature. Residual aluminium can be present in form of aluminium hydroxide or aluminium oxy hydroxide, depending on the heat treatment. α-aluminium oxide is the most thermodynamically stable form of alumina [61,62]. The high amounts of wurtzite (AlN) may play a crucial role in the foaming process as shown in the following equation [62]:

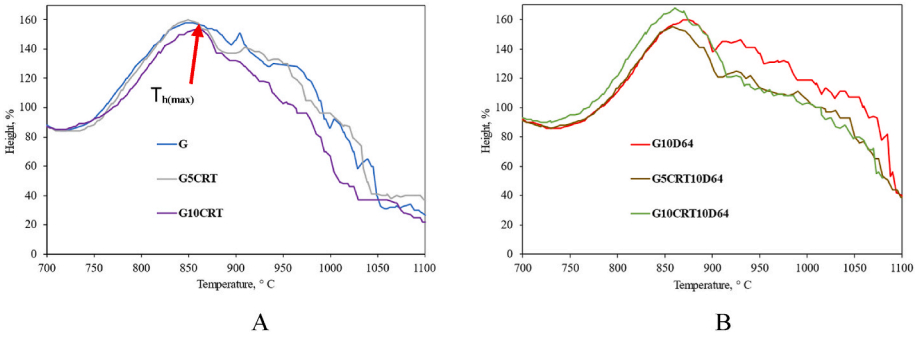

Figure 3. Heating microscopy curves of dross-free samples (A) and samples with dross (B).

$$4AlN(s)+3O_2(g) = 2Al_2O_3(s)+2N_2(g) \quad (5)$$

Table 4
Foaming characteristics: maximum height during foaming and corresponding temperature for the mixtures.

Name	h_{max} (%)	$T_{h(max)}$ (°C)
G	158	847
G5CRT	160	849
G10CRT	154	860
G10D64	160	869
G5CRT10D64	155	858
G10CRT10D64	168	860

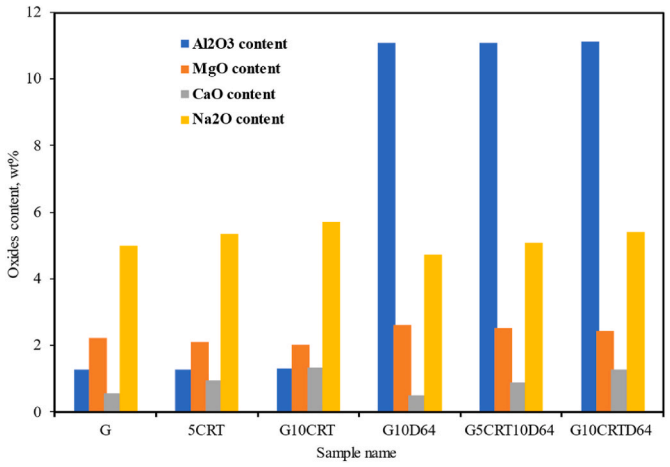

Figure 4. Al_2O_3, MgO, CaO, and Na_2O content in the samples.

3.2. Heating microscopy analysis

The foaming behavior of the mixtures can be observed in Fig. 3. Table 4 exhibits the foaming temperature chosen which corresponds to the maximum heating height recorded by the camera during sintering. In all the mixtures, the foaming temperature didn't exceed 870 °C with the foaming height ranging from 154 to 168 %. Due to the similarity of viscosity of lead glass and commercial soda-lime-silica glass (10^2 to 10^{15} P) [63], samples with only container glass and samples with 5 wt% CRT glass have similar foaming temperature (849 °C) and height (160 %). Samples with 10 wt% CRT glass have a higher foaming temperature (860 °C) which indicates a higher viscosity environment at 849 °C.

Dross-containing samples have a higher foaming height compared to the dross-free samples. Samples with the maximum CRT glass and dross content combined (G10CRT10D64) have the highest foaming height (168 %). It may be due to the self-foaming mechanism of the dross where aluminium nitride decomposes and releases gaseous products like NH_3, N_2, and NO at a temperature between 800 and 920 °C [51,57].

3.3. Cell size characterization and chemical composition of the foam glass

Foam structure (cell shape, distribution, and thickness) is the result of the viscosity during the foaming process. In vitreous silica, the elevated viscosity is attributed to the robust Si–O bonds that prevail at low temperatures. These bonds exhibit resilience and only undergo breakage at relatively high temperatures, leading to a gradual reduction in viscosity. In addition, the viscosity of soda lime silica can be significantly modified by the presence of cations and alkali contents. This will lead to the question of whether the same case can take place in the foam glass as it contains a high amount of cations and alkali content (Fig. 4). Alkali oxides like NaO can create non-bridging oxygen causing viscosity

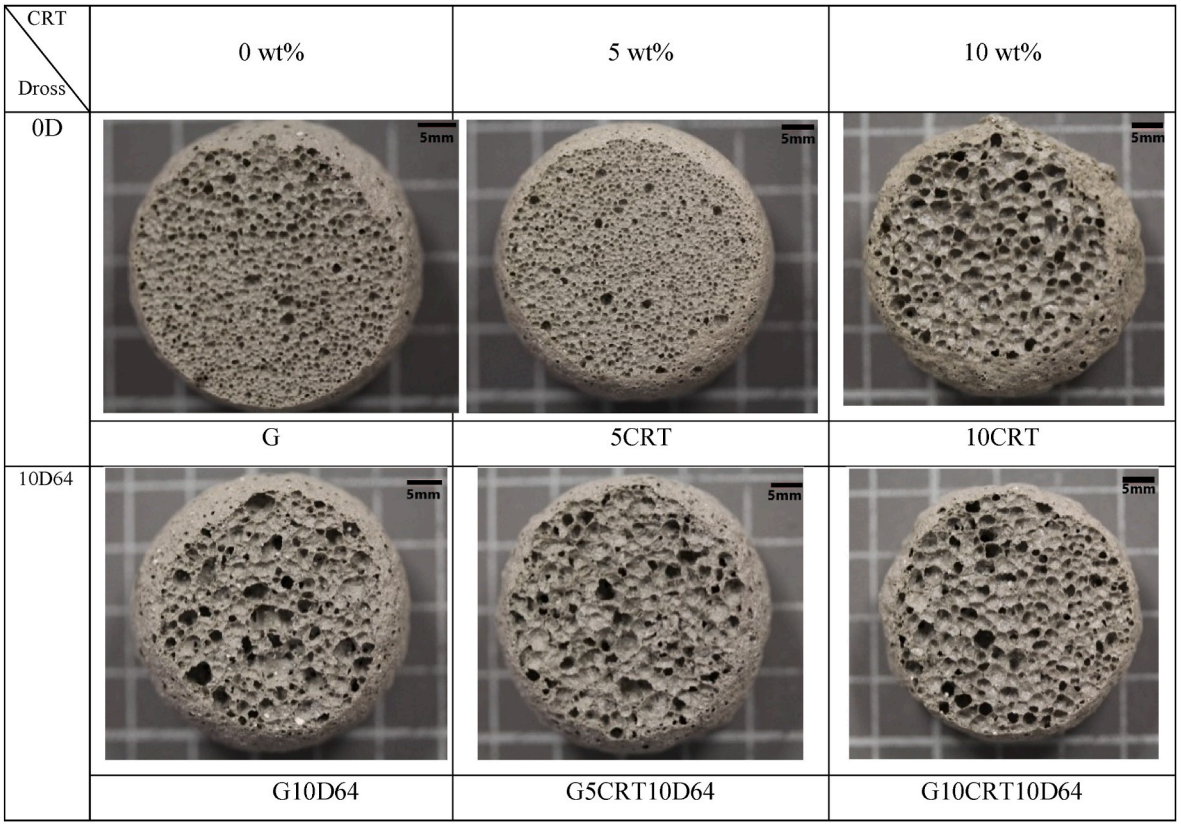

Figure 5. Macrographs of the foam glasses (scale = 5 mm).

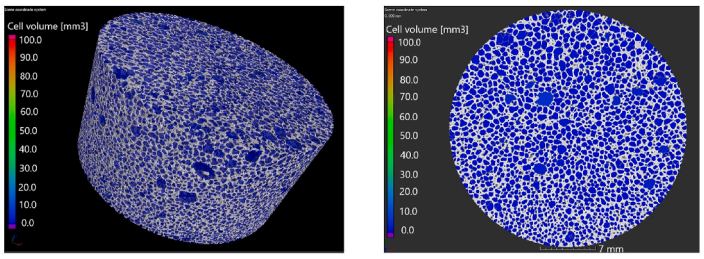

Container glass sample (**G**)

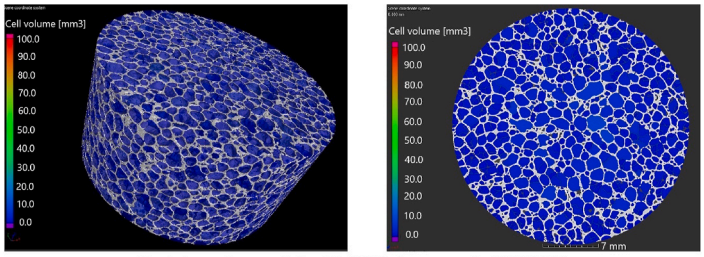

Container glass and 5 wt% CRT glass sample (**G5CRT**)

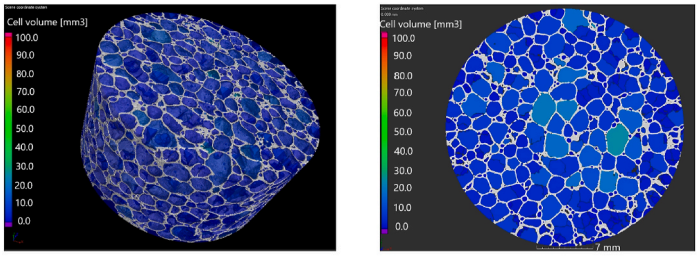

Container glass and 10 wt% CRT glass sample (**G10CRT**)

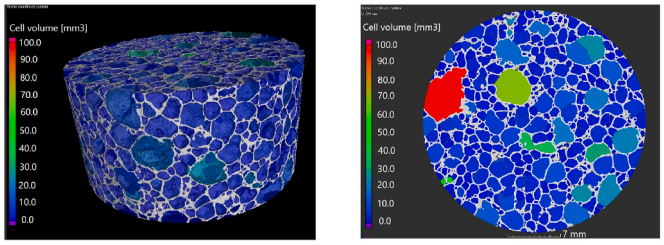

Container glass with 10 wt% dross sample (**G10D64**)

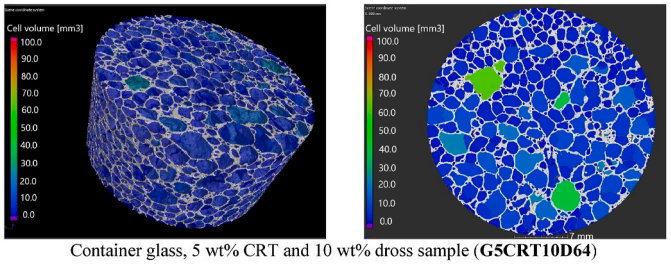

Container glass, 5 wt% CRT and 10 wt% dross sample (**G5CRT10D64**)

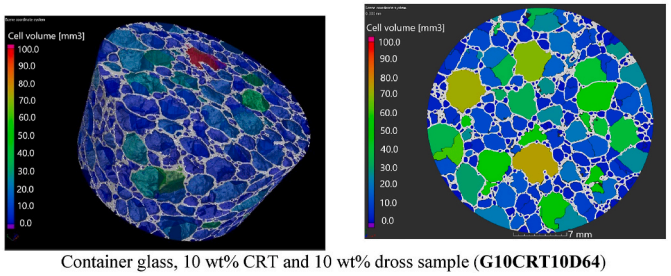

Container glass, 10 wt% CRT and 10 wt% dross sample (**G10CRT10D64**)

Figure 6. CT scans of the samples.

Table 5
Statistical parameters of the cell size distribution determined from the 2D CT scan.

	G	G5CRT	G10CRT	G10D64	G5CRT10D64	G10CRT10D64
Average (mm)	0.72	0.79	0.76	0.62	0.69	0.68
Median (mm)	0.72	0.57	0.48	0.38	0.43	0.44
Mode (mm)	0.74	0.30	0.27	0.26	0.31	0.27
Maximum (mm)	3.13	3.18	5.50	7.23	6.06	7.54
Minimum (mm)	0.16	0.14	0.13	0.02	0.13	0.03
Standard deviation	0.29	0.53	0.71	0.65	0.66	0.75

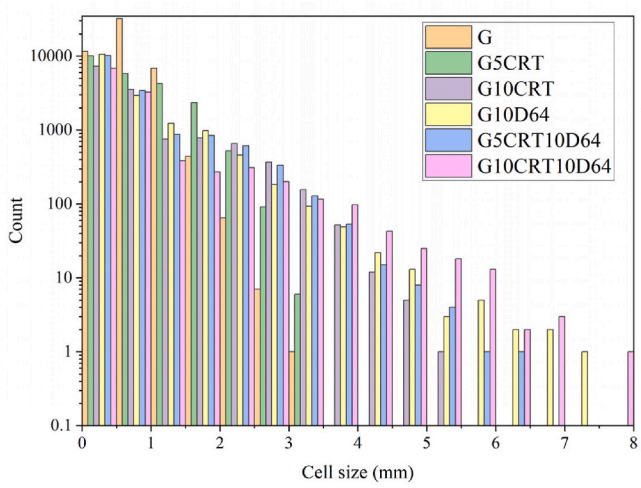

Figure 7. Cell size distributions of the samples.

to decrease. The addition of alkali earth oxide (CaO) has the same effect as NaO by loosening up the network [64]. While Na^+ and Ca^+ act as a network modifier, Mg^+ can be a network former if the formation of tetrahedrons [MgO_4] is possible by valence compensation. The same conclusion can be drawn for Al_2O_3 where [AlO_4] coordination is possible by valence compensation if enough alkali ions exist. In the absence of alkali ions, Al^{3+} ions move into the coordination of 6 and thus act as a network modifier so the viscosity falls [64].

Depending on the strength of the network modifiers, their ability to span across non-bridging oxygens increases with higher field strength, consequently limiting the reduction in viscosity. Lower temperatures are especially suitable for this effect, whereas higher temperatures are more favorable for the network modifiers with elevated field strengths to coordinate effectively. This facilitates additional relaxation of the remaining network, leading to a subsequent reduction in viscosity. Thus, the impact of network modifiers is temperature-dependent [64].

3.3.1. *Macroscopic analysis*

A comprehensive examination of the macro- and microstructure is essential to ascertain the impact of various oxides on foam glass. In Fig. 5, images of foam glass are depicted. Additionally, Fig. 6 displays 2D and 3D CT scans of the samples, along with corresponding statistical parameters (Table 5 and Fig. 7), facilitating an understanding of the structural alterations based on composition.

In container glass foams, cells exhibit a small, predominantly homogeneous hexagonal shape reminiscent of a honeycomb structure. The cell size ranges from 0.16 to 3.13 mm with an average of 0.72 mm. The standard deviation (SD) is close to 0 (0.29) reflecting the dispersion within the cell size and indicating the homogeneity of the structure while a deviation close to 1 indicates a heterogeneous structure. This cellular structure is the result of a highly viscous environment. Adding 5 wt% CRT glass results only in a marginal increase in the cell size with the average reaching 0.79 mm. Slight elevations in CaO and N_2O content contribute to this change, hinting a modest reduction in viscosity. Upon reaching a CRT glass content of 10 wt%, the maximum cell size expands to 5.5 mm, adopting an oval shape and exhibiting a heterogeneous structure (SD = 0.71). This notable increase may be attributed to the presence of a high content of Na_2O and CaO leading to the creation of non-bridging oxygens and consequent viscosity reduction. Lower viscosity will allow the creation of bigger bubbles. Thus, by adding CRT glass content the alkali oxides will increase which will lower the viscosity where the outer walls of the bubbles will collapse and merge during gas generation.

By adding aluminium dross to the container glass, sample exhibits a rother increase in the heterogeneity of the cells (SD = 0.65) with irregular cell shapes and larger-sized cells that can reach a maximum size of 7.23 mm. Simultaneously, the minimum detected cell size decreases to 0.02 mm. A similar trend is observed in the sample containing 10 wt% CRT content. Besides increasing the maximum cell size in the sample with 5 wt% CRT, the minimum cell size is higher compared to the dross-containing samples (0.13 mm). The mode indicates the cell size which occurs most often in the data set. Except for container glass samples, other samples have a small common cell size (0.2–0.3 mm), which indicates that increasing dross and CRT glass content will increase both the cell size and the number of small pores within the walls.

The aluminium oxides present in dross tend to increase the viscosity to provide a more stable structure. However, this effect is not evident here, possibly due to the foaming effect boosted by the high content of AlN in dross. This allows the fusion of the gas bubbles and the growth of big cells.

3.3.2. *Microscopic analysis*

A comprehensive analysis of the cellular system was conducted using scanning electron microscopy to provide a detailed description. Key features for foam glass characterization, including geometry, cell size, orientation, and type of connectivity, were examined (Fig. 8).

The pores were categorized into nanopores (sub-nanopore: 0.1–1 nm, inter-nanopore: 1–10 nm, and super-nanopores: 10–100 nm), micropores (sub-micropore: 0.1–1 μm, inter-micropore: 1 and 10 μm, and super-micropore: 10–100 μm), and millipores (sub-millipore: 0.1 and 1 mm, inter-millipore: 1–10 mm, and super-millipore: 10–100 mm)) [65].

Foam glass produced with container glass primarily exhibits submillipores, taking on a tetrahedrahexagon shape rather than being round. The cell walls are thin, with oval super-micropores, surrounded by thinner walls containing submicropores. Introduction of 5 wt% CRT glass results in the appearance of oval sub-millipores, surrounded by a high number of round super-micropores. Millipores, deeper than those in container glass foam, suggest potential open porosity. With the addition of 10 wt% CRT glass, slightly larger inter-millipores with organized arrangements emerge, featuring walls containing fewer super-nanopores compared to other samples.

Incorporating 10 wt% aluminium dross alters the foam glass structure. Samples with container glass and dross display inter-millipores, with walls made of inter-micropores linked together. The concave part of the pore exhibits a needle structure, indicating a possible crystallized phase. Micrographs of samples with 5 wt% CRT glass and dross show large and irregular inter-millipores, while the walls are an agglomeration of inter-to super-micropores. Samples with the same amount of dross but a higher CRT glass content exhibit a cell structure similar to

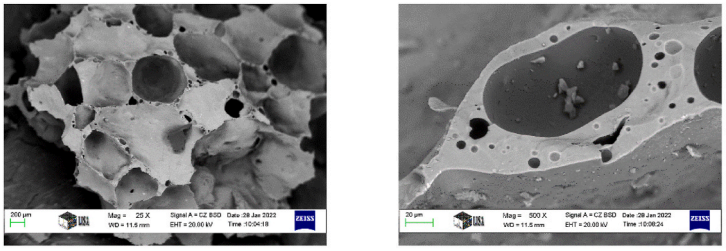

G

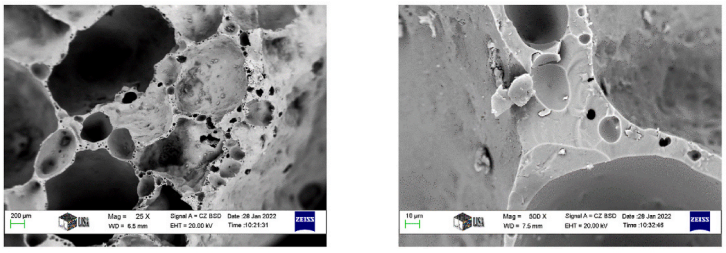

G5CRT

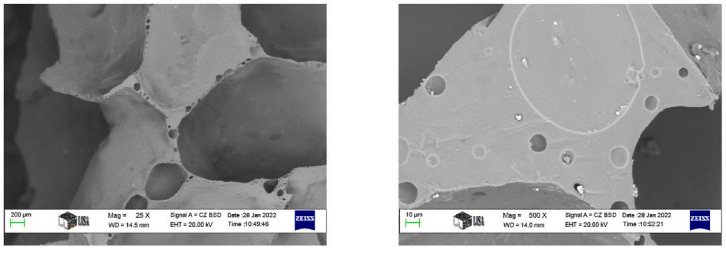

G10 CRT

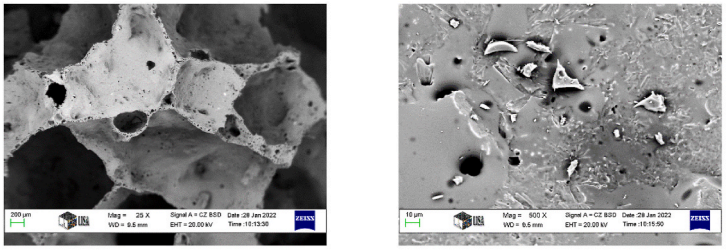

G10D64

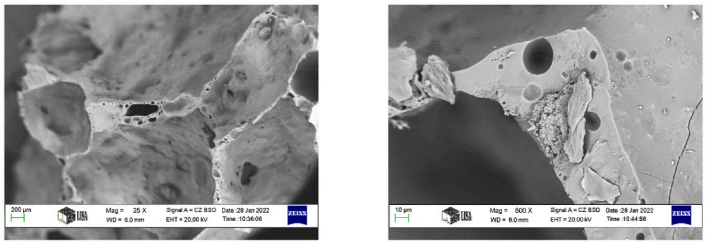

G5CRT10D64

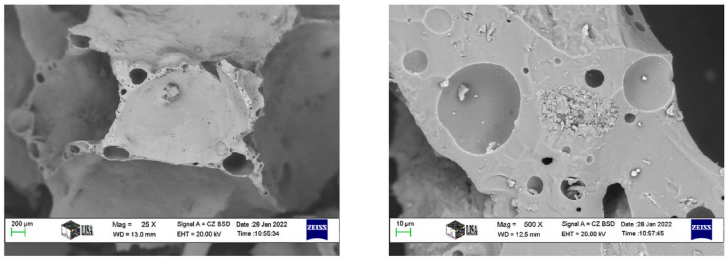

G10CRT10D64

Figure 8. Micrographs of the foam glasses.

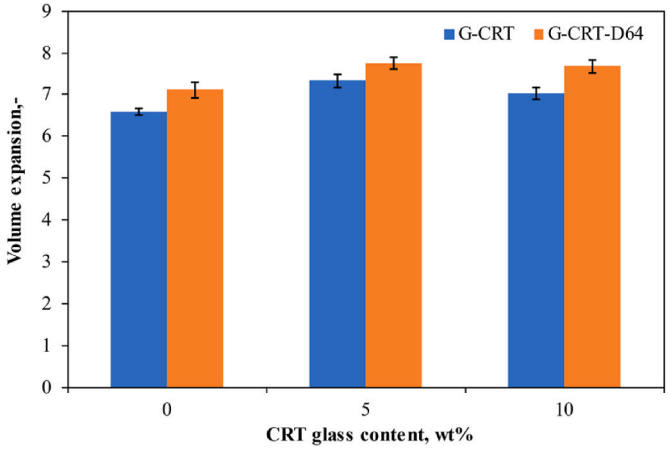

Figure 9. Volume expansion of the samples.

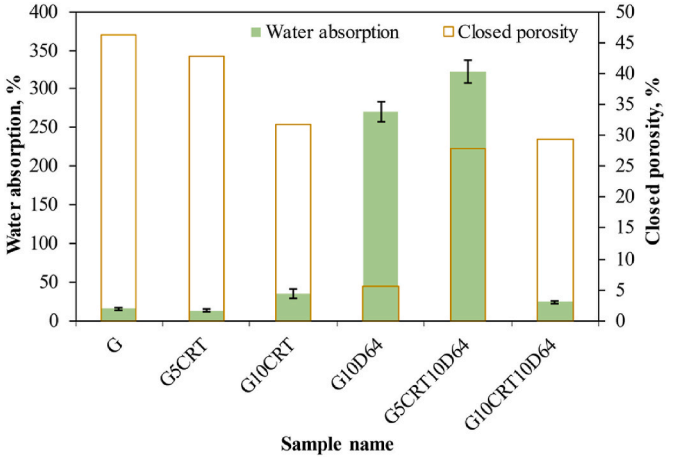

Figure 11. Water absorption versus closed porosity of the various samples.

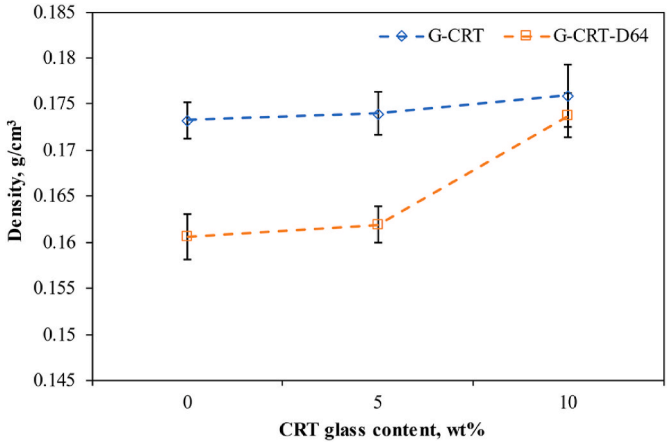

Figure 10. The density of the samples in the function of CRT content.

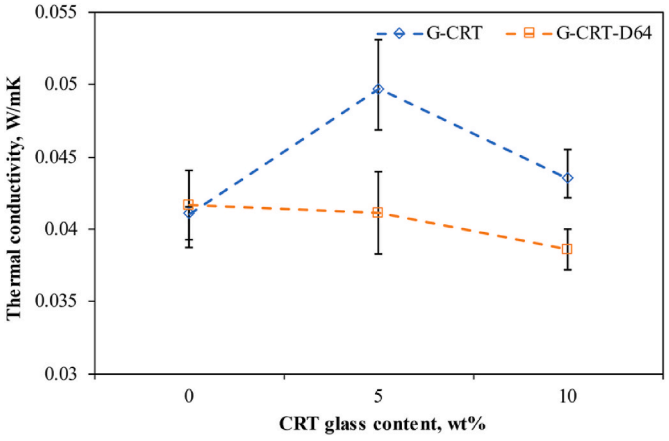

Figure 12. Thermal conductivity of the various samples.

samples with 5 wt% dross, with slightly thicker walls, despite the presence of similar inter-to super-micropores.

While AlN in dross tends to enhance foaming, causing cell fusion at a certain point, other compounds act as counter-effects by increasing viscosity, such as aluminium oxides, thereby decelerating the foaming process.

3.4. Volume expansion and density results

The calculation of volume change post-sintering involves comparing the expanded volume of the foamed sample to the initial volume of the pressed sample. Fig. 9 illustrates the outcomes of the sintering process, demonstrating significant expansion across all samples. Volume expansion offers a more precise metric than foaming height, by combining both height and diameter expansion of the sample. The highest volume expansion is observed in dross-containing samples (7.8), attributed to the presence of AlN (10.65 wt%), which enhances the foaming process. However, prioritizing a stable foam structure over maximal volume expansion is crucial. Insufficient heating or high viscosity can hinder gas bubble generation, while excessively low viscosity or intense foaming can lead to pore collapse and bubble fusion. Hence, maintaining a moderate amount of AlN in the dross and optimizing viscosity for bubble growth is essential for stable foam structure formation.

The density of foam glass is the result of the foam structure, including cell size and shape. Commercial foam glasses typically range between 0.13 and 0.3 g/cm^3 in density. In this study, foam glass densities vary from 0.15 to 0.18 g/cm^3 (Fig. 10). Dross-free samples exhibit slightly higher densities compared to those with dross, attributable to increased cell size upon dross addition.

3.5. Water absorption and closed porosity

Foam glass exhibits versatile characteristics depending on its intended application. It can serve as a water-resistant material while still being able to absorb mist and humidity, or as a highly absorbent material utilized for drainage purposes. Closed pores, exemplified by dross-free samples, showcase minimal absorption, with pure container glass demonstrating the lowest absorption rate at 15 % (Fig. 11). Introducing 5 or 10 wt% CRT glass slightly elevates water absorption to 30 wt%. If we compare the latest cell microstructure, there is a relevant resemblance. This is probably due to the limited amount of gaseous substances generated during foaming. Open porosity typically results in high water absorption, exceeding 300 %. This trend is observed in samples containing 5 wt% CRT and dross while samples with 10 wt% CRT and dross show a low absorption rate (24 %). The high absorption in sample G5CRT10D64 is may due to the microstructure of the pores where the cells seem irregular with interconnected pores and ink-bottle pores which allowed water to accumulate inside the sample. It is explained by the gas bubble not being able to sustain its form during foaming causing the walls to collapse and merge. Incorporating 10 wt% CRT glass into the dross aids in stabilizing the pore structure and restraining the foaming process.

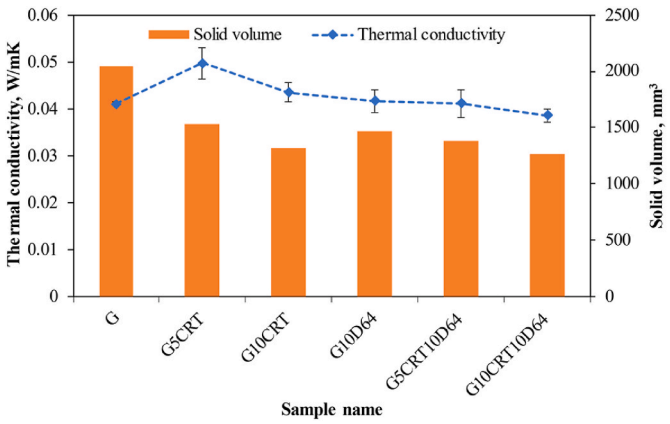

Figure 13. Effect of the solid volume of the samples on the thermal conductivity.

3.6. Thermal resistance

The thermal conductivity of commercial foam glass typically falls within the range of 0.035–0.08 W/m•K [2–4]. In this investigation, the thermal conductivity of the samples ranges from 0.038 W/m•K to 0.05 W/m•K (Fig. 12), rendering them effective thermal insulators.

Samples with open pores and higher water absorption exhibit lower thermal conductivity compared to those with closed cells. Factors such as cell size, wall thickness, and uniformity directly influence thermal conductivity. The homogeneity of the foam glass structure, indicated by the standard deviation, plays a crucial role in thermal resistance. A heterogeneous cell size distribution typically results in better thermal resistance. Notably, G10CRTD64 foam glass, characterized by a heterogeneous cell structure (SD = 0.7), displays the lowest thermal conductivity. In this context, Heat transfer through foam occurs via four mechanisms: conduction through the solid phase, conduction through the gas phase, convection, and radiative exchange. If the temperature differences between the fluid and the solid cell edges are small at the scale of a cell, natural convection within the cells is considered negligible [66]. In this case, heat flow predominantly occurs through solids, particularly through the walls. Thin walls containing a high number of pores attenuate heat flow effectively. It can be seen in Fig. 13, which presents the carcass or solid volume of the foam glass determined by computed tomography. If we exclude the foam glass made by only container glass (G), we can see that as the solid volume decreases the thermal conductivity decreases. This behavior can be observed in samples with dross content.

3.7. Comparison between the resultant foam glass properties and that of the previous literature

As previously noted, foam glass can be manufactured using a variety of waste materials. However, research indicates that despite utilizing similar starting materials, the resultant foam products often exhibit divergent properties owing to disparities in foaming conditions and additives employed. Table 6 provides a comprehensive comparison of foam glass products derived from identical or closely related starting materials.

4. Conclusions

Foam glass was successfully synthesized using 100 % waste materials, including container glass, cathode ray tube (CRT) glass (5 and 10 wt%), secondary aluminium dross (10 wt%), and silicon carbide (2 wt %). The resultant foam glass exhibited properties comparable to commercial counterparts. Key findings include:

- The produced foam glass demonstrated a lightweight property, boasting a density ranging from 0.15 to 0.18 g/cm^3. The addition of aluminium dross notably enhanced the foaming potential of the glass powder, attributed to the self-foaming mechanism of the dross wherein aluminium nitride decomposes, liberating gaseous byproducts.
- Alkali content exerted a similar influence on foam glass viscosity as observed in soda lime glass, with NaO and CaO functioning as network modifiers, leading to a reduction in viscosity by generating non-bridging oxygen. Despite the aluminium oxides in the dross potentially increasing viscosity to confer structural stability, this effect was mitigated, possibly due to the heightened foaming propensity facilitated by the AlN content in the dross. Consequently, gas bubble fusion and the formation of larger cells were created.
- The resulting foam glass showcased low thermal conductivity (ranging from 0.038 W/m·K to 0.05 W/m·K), attributable to the heterogeneous distribution of cells, which effectively attenuated heat convection. This characteristic renders them highly effective as thermal insulators. Additionally, foam glasses with both high

Table 6
Comparison of this research results to previous literature in glass ceramics with close compositions.

Researcher	Materials	Volume expansion (−)	Water absorption (%)	Apparent density (g/cm^3)	Total Porosity (%)	Open Porosity (%)	Thermal conductivity (Wm^{-1} K^{-1})
This research	Container glass	6.58	15.43	0.17	92.33	46.11	0.04
König et al. [36]	container glass + carbon black + iron oxide	–	–	0.12–0.14	94.5–95.5	91.2–98.6	0.057–0.065
Da Costa et al. [67]	87.5 wt% container glass + 2.5 wt% bentonite	–	12.1–24.1	1.55–1.57	18.8–37.7	–	–
This research	Container glass + CRT glass	7	13.30–35.13	0.17–0.18	92–93	49–61.2	0.04–0.05
König et al. [36]	CRT glass + carbon black + Manganese oxide	–	–	0.1–0.24	91.3–96.2	0–8	0.037–0.049
Hribar et al. [68]	CRT glass +Mn_3O_4 + carbon	–	–	0.13–0.18	94–95	8–29	0.041–0.054
This research	Container glass + aluminium dross	6–8	270	0.16	93	88	0.04
	Container glass + CRT glass + aluminium dross	6–8	24–322	0.16–0.17	91–93	63–66	0.038–0.04
Zhang et al. [69]	Municipal waste incineration bottom ash + fly ash + pickling sludge + secondary aluminum ash	–	4.03–16.55	1.51–1.68	57.9–62.2	–	–
El Amir et al. [57]	Container glass + aluminium dross (7 wt%)	–	–	0.15–0.6	80-92 vol%	–	0.11–0.21
Da Silva et al. [70]	Container glass + alumina	–	10–60	0.4–1.5	57–85	–	–

absorption (open porosity) and low absorption (closed porosity) were produced. Foam glass with closed porosity holds promise as insulation material for housing and building applications, while samples with open porosity find utility in filtration systems.

CRediT authorship contribution statement

Meriem Sassi: Writing – original draft, Methodology, Investigation. **Andrea Simon:** Writing – review & editing, Project administration. **Sindy Fuhrmann:** Validation, Methodology. **Stephan A.H. Sander:** Investigation. **Roland Szabó:** Investigation.

Declaration of competing interest

The authors declare that they have no known competing financial interests or personal relationships that could have appeared to influence the work reported in this paper.

Acknowledgments

The authors gratefully acknowledge the support provided by Daniella Ipari Park Ltd. and Arconic-Kőfém Mill Products Hungary Ltd. Additionally, special thanks go to Tamas Kekesi, Karoly Gal, Istvan Kocserha, Oliver Banhidi, and Ferencz Móricz for their assistance in the pretreatment of the dross, heating microscopy, XRD, and XRF, respectively.

References

[1] M. Sassi, A. Simon, Waste-to-Reuse foam glasses produced from soda-lime-silicate glass, cathode ray tube glass, and aluminium dross, INORGA 10 (1) (2021).
[2] N. Karandashova, B. Goltsman, E. Yatsenko, Analysis of influence of foaming mixture components on structure and properties of foam glass, in: *IOP Conf. Series: Materials Science And Engineering*, Novocherkassk, 2017.
[3] H. Wang, Z. Chen, R. Ji, L. Liu, X. Wang, Integrated utilization of high alumina fly ash for synthesis of foam glass ceramic, Ceram. Int. 44 (12) (2018) 13681–13688.
[4] C. Xi, F. Zheng, X. Jiahe, W. Yang, Y. Peng, Y. Li, P. Li, Q. Zhen, Preparation of glass-ceramic foams using extracted titanium tailing and glass waste as raw materials, Construct. Build. Mater. 190 (2018) 896–909.
[5] C. Arriagada, I. Navarrete, M. Lopez, Understanding the effect of porosity on the mechanical and thermal performance of glass foam lightweight aggregates and the influence of production factors, Construct. Build. Mater. 228 (2019) 116746.
[6] D. Bozsaky, The historical development of thermal insulation materials, Periodica Polytechnica Architecture 41 (2) (7 April 2017) 49–56.
[7] P.C. Román, J.V. Calvo, A.L. Gil, J. König, M.Á. Rodríguez-Perez, Modelling of the mechanisms of heat transfer in recycled glass foams, Construct. Build. Mater. 274 (2021) 122000.
[8] L. Hu, F. Bu, F. Guo, Z. Zhang, Construction method of foam glass thermal insulation material in sloping roof, IOP Conf. Ser. Earth Environ. Sci. 61 (2017) 012122.
[9] Foamit, Foamit, applications for civil engineering [Online], http://www.foamit.fi/wp-content/uploads/2016/10/Foamedglass.pdf, 2019, 15 februry 2019.
[10] W.S. Mustafa, B. Nagy, J. Szendefy, Impact of compaction ratio, loading period and environmental condition on compressional behavior of foam glass aggregate, Construct. Build. Mater. 343 (2022) 128111.
[11] Y. Attila, M. Guden, A. Tasdemirci, Foam glass processing using a polishing glass powder residue, Elsevier Ceramics International 39 (2013) 5869–5877.
[12] R.C. Da Silvaa, E.T. Kubaski, E.T. Tenório-Neto, M.K. Lima-Tenório, S. M. Tebcherani, Foam glass using sodium hydroxide as foaming agent: study on the reaction mechanism in soda-lime glass matrix, J. Non-Cryst. Solids 511 (2019) 177–182.
[13] A. Rincon, D. Desideri, E. Bernardo, Functional glass-ceramic foams from 'inorganic gel casting' and sintering of glass/slag mixtures, J. Clean. Prod. 187 (2018) 250–256.
[14] D. Tulyaganov, H. Fernandes, S. Agathopoulos, J. Ferreira, Preparation and characterization of high compressive strength foams from sheet glass, J. Porous Mater. 13 (2006) 33–139.
[15] S.S. Owoeye, G.O. Matthew, F.O. Ovienmhanda, S.O. Tunmilayo, Preparation and characterization of foam glass from waste container glasses and water glass for application in thermal insulations, Ceram. Int. 46 (8) (2020) 11770–11775.
[16] J. König, V. Nemanič, M. Žumer, R.R. Petersen, M.B. Østergaard, Y. Yue, D. Suvorov, Evaluation of the contributions to the effective thermal conductivity of an open-porous-type foamed glass, Construct. Build. Mater. 214 (2019) 337–343.
[17] R. Ji, Y. Zheng, Z. Zou, Z. Chen, S. Wei, X. Jin, M. Zhang, Utilization of mineral wool waste and waste glass for synthesis of foam glass at low temperature, Construct. Build. Mater. 2015 (2019) 623–632.
[18] Z. Chen, H. Wang, R. Ji, L. Liu, C. Cheeseman, X. Wang, Reuse of mineral wool waste and recycled glass in ceramic foams, Ceram. Int. 45 (2019) 15057–15064.
[19] L. Yang, Z. Shili, M. Shuhua, L. Chunli, W. Xiaohui, Preparation of sintered foamed ceramics derived entirely from coal fly ash, Construct. Build. Mater. 163 (2018) 529–538.
[20] D. Baidzhanov, Z.S. Nuguzhinov, F.V. I, P.A. Kropachev, Thermal insulation material based on local technogenic raw material, Glass Ceram. 73 (11 – 12) (2016) 427–430.
[21] Q. Ma, Q. Wang, L. Luo, F. Chaozhen, Preparation of high strength and low-cost glass ceramic foams, IOP 52 (39) (2018).
[22] Q. Zipeng, G. Li, Y. Tian, M.a.P.S. Yuwei, Numerical simulation of thermal conductivity of foam glass based on the steady-state method, MD 12 (1) (2018) 54.
[23] J. Li, X. Zhuang, E. Monfort, X. Querol, A.S. Llaudis, O. Font, N. Moreno, F. J. García Ten, I. Maria, Utilization of coal fly ash from a Chinese power plant for manufacturing highly insulating foam glass: implications of physical, mechanical properties and environmental features, Elsevier, Construction and Building Materials 175 (2018) 64–76.
[24] L. Taoyong, L. Piao, G. Xiaogang, Z. Jiashuo, H. Qianxing, L. Zhiwei, X. Zhou, Y. Qifeng, T. Yougen, L. Anxian, Preparation, characterization and discussion of glass ceramic foammaterial: analysis of glass phase, fractal dimension and self-foaming mechanism, Mater. Chem. Phys. 243 (2020) 122614.
[25] M. Pavlíková, A. Pivák, M. Záleská, A.-M. Lauermannová, F. Antončík, M. Lojka, O. Jankovský, Z. Pavlík, Assessment of wood chips ash as efficient admixture in foamed glass-MOC composites, J. Mater. Res. Technol. 19 (2022) 2287–2300.
[26] V. Cosmin, I. Lazău, Glass foam from window panes and bottle glass wastes, Cent. Eur. J. Chem. 12 (2013) 804–811.
[27] H. Shi, K.-q. Feng, H.-b. Wang, C.-h. Chen, H.-l. Zhou, Influence of aluminium nitride as a foaming agent on the preparation of foam, Int. J. Miner. Metall. Mater. 23 (5) (2016) 595.
[28] L. Taoyong, L. Changwei, L. Jianlei, H. Lei, G. Hua, L. Cui, Z. Xin, T. Hui, Y. Qifeng, L. Anxian, Phase evolution, pore morphology and microstructure of glass ceramic foams derived from tailings wastes, Ceram. Int. 44 (2018) 14393–14400.
[29] G. Yuxi, Z. Yihe, H. Hongwei, M. Ke, H. Kunran, H. Pan, X. Wang, Z. Zhilei, M. Xianghai, Novel glass ceramic foams materials based on red mud, Ceram. Int. 40 (2014) 6677–6683.
[30] C. Bai, H. Li, E. Bernardo, P. Colombo, Waste-to-resource preparation of glass-containing foams from geopolymers, Ceram. Int. 45 (2019) 7196–7202.
[31] M. Mahinroosta, A. Allahverdi, Hazardous aluminum dross characterization and recycling strategies: acritical review, J. Environ. Manag. 223 (2018) 452–468.
[32] F. Méar, P. Yot, M. Cambon, M. Ribes, The characterization of waste cathode-ray tube glass, Waste Manag. 26 (12) (2006) 1468–1476.
[33] E. Bernardo, G. Scarinci, S. Hreglich, G. Zangiacomi, Effect of time and furnace atmosphere on the sintering of glasses from dismantled cathode ray tubes, J. Eur. Ceram. Soc. 27 (2–3) (2007) 1637–1643.
[34] E. Restrepo, R. Widmer, M. Schluep, Leaded Glass from Cathode Ray Tubes (CRTs): A Critical Review of Recycling and Disposal Options, United Nations University, Bonn, 2016.
[35] Y. Qi, X. Xiao, Y. Lu, J. Shu, J. Wang, M. Chen, Cathode ray tubes glass recycling: a review, Sci. Total Environ. 650 (Part 2) (2019) 2842–2849.
[36] J. König, A. Lopez-Gil, P. Cimavilla-Roman, M.A. Rodriguez-Perez, R.R. Petersen, M.B. Østergaard, N. Iversen, Y. Yue, S. Matjaz, Synthesis and properties of open- and closed-porous foamed glass with a low density, Construct. Build. Mater. 247 (2020) 118574.
[37] M.B. Østergaard, R.R. Petersen, J. König, Y. Yue, Effect of alkali phosphate content on foaming of CRT panel glass using Mn3O4 and carbon as foaming agents, J. Non-Cryst. Solids 482 (2018) 217–222.
[38] M.B. Østergaard, M. Zhang, X. Shen, R.R. Petersen, J. König, P.D. Lee, Y. Yue, B. Cai, High-speed synchrotron X-ray imaging of glass foaming and thermal conductivity simulation, Acta Mater. 189 (2020) 85–92.
[39] M.B. Østergaard, R.R. Petersen, K. Jakob, M. Bockowski, Y. Yue, Impact of gas composition on thermal conductivity of glass foams prepared via high-pressure sintering, J. Non-Cryst. Solids: X 1 1 (2019) 100014.
[40] H.R. Fernandes, D.D. Ferreira, F. Andreola, I. Lancellotti, L. Barbieri, J.M. Ferreira, Environmental friendly management of CRT glass by foaming with waste egg shells, calcite or dolomite, Ceram. Int. 40 (8) (2014) 13371–13379. Part B.
[41] J. König, R.R. Petersen, Y. Yue, Fabrication of highly insulating foam glass made from CRT panel glass, Ceram. Int. 41 (8) (2015) 9793–9800.
[42] P. Tsakiridis, Aluminium salt slag characterization and utilization – a review, J. Hazard Mater. 217–218 (2012) 1–10.
[43] P. Tsakiridis, P. Oustadakis, S. Agatzini-Leonardou, Aluminium recovery during black dross hydrothermal treatment, J. Environ. Chem. Eng. 1 (1–2) (2013) 23–32.
[44] A. Kudyba, S. Akhtar, I. Johansen, J. Safarian, Aluminum recovery from white aluminum dross by a mechanically activated phase separation and remelting process, J. Miner. Met. Mater. Soc. 73 (9) (2021) 2625–2634.
[45] Y. Li, Q. Ziyi, L. Chunlei, Q. Yi, W. Haibin, P. Li, W. Yi, Hazardous characteristics and transformation mechanism in hydrometallurgical disposing strategy of secondary aluminum dross, J. Environ. Chem. Eng. 9 (6) (2021) 106470.
[46] A. Meshram, R. Jha, S. Varghese, Towards recycling: understanding the modern approach to recover waste aluminium dross, Mater. Today: Proc. 46 (Part 3) (2021) 1487–1491.
[47] P. Ramaswamy, P. Tilleti, S. Bhattacharjee, R. Pinto, S.A. Gomes, Synthesis of value added refractories from aluminium dross and zirconia composites, Mater. Today: Proc. 22 (part 4) (2020) 1264–1273.
[48] G. Qin, G. Qiang, L. Yongli, R. Baozeng, F. Mingbo, L. Huilin, T. Dengchao, D. Min, Innovative technology for defluorination of secondary aluminum dross by alkali leaching, Miner. Eng. 172 (2021) 107134.

[49] A. Tripathy, S. Mahalik, C. Sarangi, B. Tripathy, K. Sanjay, I. Bhattacharya, A pyro-hydrometallurgical process for the recovery of alumina from waste aluminium dross, Miner. Eng. 137 (2019) 181–186.
[50] Z. Zhengping, L. Han, R. Li, L. Fengqin, Z. Hongliang, A new approach to recover the valuable elements in black aluminum dross, Resour. Conserv. Recycl. 174 (2021) 105768.
[51] H. Shen, B. Liu, Z. Shi, S. Zhao, J. Zhang, S. Zhang, Reduction for heavy metals in pickling sludge with aluminum nitride in secondary aluminum dross by pyrometallurgy, followed by glass ceramics manufacture, J. Hazard Mater. 418 (2021) 126331.
[52] H. Lv, M. Xie, L. Shi, H. Zhao, Z. Wu, L. Li, R. Li, F. Liu, A novel green process for the synthesis of high-whiteness and ultrafine aluminum hydroxide powder from secondary aluminum dross, Ceram. Int. 48 (1) (2022) 953–962.
[53] H. Shen, B. Liu, C. Ekberg, S. Zhang, Harmless disposal and resource utilization for secondary aluminium dross: a review, Sci. Total Environ. 760 (2021) 143968.
[54] Q. Li, Q. Yang, G. Zhang, Q. Shi, Investigations on the hydrolysis behavior of AlN in the leaching process of secondary aluminum dross, Hydrometallurgy 182 (2018) 121–127.
[55] K.V. Shailendra, K.D. Vijay, P.D. Shashi, Utilization of aluminium dross for the development of valuable product – a review, Mater. Today: Proceedings, Vols 43 (Part 1) (2021) 547–550.
[56] N.A. Roslan, S.Z. Abidina, O.U. Osazuwa, S.Y. Chin, Y. Taufiq-Yap, Int. J. Hydrogen Energy 46 (60) (2021) 30959–30975.
[57] A.A. El-Amir, M.A. Attia, M. Newishy, T. Fend, M. Emad, Aluminium dross/soda lime glass waste-derived high-quality glass foam, J. Mater. Res. Technol. 15 (2021) 4940–4948.
[58] M. Sassi, J.-E.F.M. Ibrahim, A. Simon, Characterization of foam glass produced from waste CRT glass and aluminium dross, in: *Journal Of Physics Conference Series*, Miskolc, 2020.
[59] y.I. Illés, M. Sassi, H. Zakiyya, T. Kékesi, Fluoride salts from secondary aluminium DrossThe fundamental kinetic characteristics of aqueous dissolution of chloride and, in: *International Multidisciplinary Scientific Conference* , Miskolc, 2019.
[60] "Insulation," C-THERM, [Online]. Available: https://ctherm.com/applications/insulation/. [Accessed 9 June 2024].
[61] J. Cotton, "AZO Material," [Online]. Available: https://www.azom.com/article.aspx?ArticleID=1389.
[62] J. König, R.R. Petersen, Y. Yue, Influence of the glass–calcium carbonate mixture's characteristics on the foaming process and the properties of the foam glass, J. Eur. Ceram. Soc. (2014) 1591–1598.
[63] Glass Viscosity Calculation," [Online]. Available: https://glassproperties.com/viscosity/. [Accessed 1 November 2021].
[64] H. Scholze, Glass, Springer, 1991.
[65] T. Mays, A new classification of pore sizes, Stud. Surf. Sci. Catal. 160 (2007) 57–62.
[66] A.C.A. Asséko, B. Cosson, C. Duborper, M.-F. Lacrampe, Numerical analysis of effective thermal conductivity of plastic foams, J. Mater. Sci. 51 (2016) 9217–9228.
[67] F.P. Da Costa, C.R.d.S. Morais, A.M. Rodrigues, Sustainable glass-ceramic foams manufactured from waste glass bottles and bentonite, Ceram. Int. 46 (11 Part A) (2021) 17957–17961.
[68] U. Hribar, M. Spreitzer, J. König, Applicability of water glass for the transfer of the glass-foaming process from controlled to air atmosphere, J. Clean. Prod. 282 (0959–6526) (2021) 125428.
[69] J. Zhang, B. Liu, S. Zhao, H. Shen, J. Liu, S. Zhang, Preparation and characterization of glass ceramic foams based on municipal solid waste incineration ashes using secondary aluminum ash as foaming agent, Construct. Build. Mater. 262 (2020) 120781.
[70] F.P. Da Costa, C.R.d.S. Morais, H.C. Pinto, A.M. Rodrigues, Microstructure and physico-mechanical properties of Al2O3-doped sustainable glass-ceramic foams, Mater. Chem. Phys. 256 (2020) 123612.